Inorg. Chem. **2007**, *46*, 3984–3995

Molecular Tectonics of Mixed-Ligand Metal–Organic Frameworks: Positional Isomeric Effect, Metal-Directed Assembly, and Structural Diversification

Miao Du,* Xiu-Juan Jiang, and Xiao-Jun Zhao

College of Chemistry and Life Science, Tianjin Normal University, Tianjin 300074, P. R. China

Received November 3, 2006

A series of nine mixed-ligand metal–organic frameworks (MOFs) have been prepared by the combination of a bent dipyridyl linker 4-amino-3,5-bis(4-pyridyl)-1,2,4-triazole (bpt) and three benzenedicarboxylate isomers (pa = phthalate, ip = isophthalate, and tp = terephthalate), respectively, with different metal ions such as Co^{II}, Ni^{II}, Cu^{II}, Zn^{II}, and Cd^{II}. The framework structures of these neutral polymeric complexes have been determined by the X-ray single-crystal diffraction technique. Structural analysis reveals that the benzenedicarboxylate isomers display versatile coordination modes to manage the metal ions to form 1-D chain or ribbon arrays, which are further extended via the exo-bidentate bpt connectors to give rise to a variety of coordination networks, such as a simple (4,4) layer, 2-D double layer with decorated (4,4) topology, 2-D layer with decorated (3,6) topology, 2-D bilayer with $8^2.10$ topology (2-fold interpenetration), 3-D polythreaded architecture (1-D + 2-D), and 2-fold interpenetrating porous lattice of (4,4) layers. The accessorial secondary interactions such as hydrogen bonding and/or aromatic stacking are also helpful for the extension and stabilization of the final supramolecular aggregates. This work evidently indicates that the isomeric effect of the anionic benzenedicarboxylate is significant in the construction of these network structures, which are also well regulated by the metal centers. The Zn^{II} and Cd^{II} MOFs exhibit strong solid-state luminescence emissions at room temperature, which originate differently from intraligand transition or ligand-to-metal charge transfer. Thermal stability of these crystalline materials has been explored by thermogravimetric analysis of mass loss. The 3-D host frameworks of MOFs **8** and **9** show similar porous cavities, and their desorption/adsorption behaviors of guest solvents have also been investigated.

Introduction

During the past decade, the rational engineering and preparation of metal−organic frameworks (MOFs) or coordination polymers with well-regulated network structures has attracted increasing interests for the sake of developing new functional materials with potential applications in the fields of catalysis, gas absorption, nonlinear optics, ion-exchange, luminescence, magnetism and so on.[1−3] In principle, the extended coordination framework solids with desired structural features and/or physicochemical properties greatly depend on the nature of the organic ligands (spacers) and metal ions (nodes). As a consequence, nowadays, utilizing suitable organic tectons with functional groups that are

* To whom correspondence should be addressed. E-mail: dumiao@public.tpt.tj.cn. Phone: 86-22-23538221. Fax: 86-22-23540315.

(1) (a) Moulton, B.; Zaworotko, M. J. *Chem. Rev.* **2001**, *101*, 1629. (b) Evans, O. R.; Lin, W. *Acc. Chem. Res.* **2002**, *35*, 511. (c) Janiak, C. *Dalton Trans.* **2003**, 2781. (d) Carlucci, L.; Ciani, G.; Proserpio, D. M. *Coord. Chem. Rev.* **2003**, *246*, 247. (e) Yaghi, O. M.; O'Keeffe, M.; Ockwing, N. W.; Chae, H. K.; Eddaoudi, M.; Kim, J. *Nature* **2003**, *423*, 705. (f) James, S. L. *Chem. Soc. Rev.* **2003**, *32*, 276. (g) Batten, S. R.; Murray, K. S. *Coord. Chem. Rev.* **2003**, *246*, 103.

(2) (a) Eddaoudi, M.; Moler, D. B.; Li, H.; Chen, B.; Reineke, T.; O'Keeffe, M.; Yaghi, O. M. *Acc. Chem. Res.* **2001**, *34*, 319. (b) Kesanli, B.; Lin, W. *Coord. Chem. Rev.* **2003**, *246*, 305. (c) Kitagawa, S.; Kitaura, R.; Noro, S. *Angew. Chem., Int. Ed.* **2004**, *43*, 2334. (d) Ockwig, N. W.; Delgado-Friederichs, O.; O'Keeffe, M.; Yaghi, O. M. *Acc. Chem. Res.* **2005**, *38*, 176. (e) Rowsell, J. L. C.; Yaghi, O. M. *Angew. Chem., Int. Ed.* **2005**, *44*, 4670. (f) Coronado, E.; Gatteschi, D. *J. Mater. Chem.* **2006**, *16*, 2513.

(3) (a) Würthner, F.; Sautter, A. *Chem. Commun.* **2000**, 445. (b) Xiong, R.-G.; Xue, X.; Zhao, H.; You, X.-Z.; Abrahams, B. F.; Xue, Z.-L. *Angew. Chem., Int. Ed.* **2002**, *41*, 3800. (c) Tong, M.-L.; Kitagawa, S.; Chang, H. C.; Ohba, M. *Chem. Commun*. **2004**, 418. (d) Takamizawa, S.; Nakata, E.; Saito, T. *Angew. Chem., Int. Ed.* **2004**, *43*, 1368. (e) Du, M.; Zhao, X.-J.; Guo, J.-H.; Batten, S. R. *Chem. Commun.* **2005**, 4836. (f) Zhao, W.; Song, Y.; Okamura, T. A.; Fan, J.; Sun, W.-Y.; Ueyama, N. *Inorg. Chem.* **2005**, *44*, 3330. (g) Wang, X.-Y.; Wang, L.; Wang, Z.-M.; Gao, S. *J. Am. Chem. Soc.* **2006**, *128*, 674. (h) Zou, R.-Q.; Sakurai, H.; Xu, Q. *Angew. Chem., Int. Ed.* **2006**, *45*, 2542.

10.1021/ic062098+ CCC: $37.00
Published on Web 04/14/2007

capable of bridging metal centers to construct such tailored crystalline materials has revealed to be a fast developing field of multidisciplinary research, being in connection with crystal engineering, coordination chemistry, supramolecular chemistry, and material science, etc.[4−6]

In this regard, coordination polymers on the basis of polycarboxylate connectors have been extensively focused due to the versatile coordination capability as well as the sensitive character to acidity of such building blocks,[7−10] which will be responsible for structural diversity of the resultant robust coordination frameworks. Among them, rigid dicarboxylate species with different orientations of the functional groups such as phthalate (pa), isophthalate (ip), and terephthalate (tp) have been widely used.[7] First, these phenyl dicarboxylate isomers contain two carboxyl groups at distinct positions, which may engender significant spatial effect and thus influence the structural assembly with multiform coordination fashions. Second, they can provide directional conformation of network structures via dative bonds and also noncovalent cooperative forces such as hydrogen bonding and/or aromatic stacking. Finally, the deprotonated carboxyl groups generally act as anionic organic ligands to complete the metal coordination as well as compensate the charge. Therefore, the metal binding tendency may be predicted to some extent, and the influence of inorganic counter anions on the framework structures will be mostly eliminated to make it more facile for structural forecast. To this day, a variety of metal−phenyl dicarboxylate frameworks have been reported; however, a systemic study of the isomeric effect on the generation of such coordination frameworks is surprisingly quite scarce.[11] With this understanding, one crucial aim of this work is to explore the essential factors of these positional isomeric tectons for regulating the structural assembly, which may provide further insights in designing new hybrid crystalline materials.

As for the dipyridyl bridging ligands, some analogous linkers derived from the proper modification of the classical 4,4′-bipyridine molecule have been employed recently, which exhibit dissimilar backbone flexibility and thus give rise to profoundly steric effect on the direction of unexpected coordination architectures upon metal complexation.[12] In our recent research, we have concentrated on the construction of mixed-ligand metal−organic frameworks based on an angular dipyridyl derivative 4-amino-3,5-bis(4-pyridyl)-1,2,4-triazole (bpt) and polycarboxylate species. For example, metal-directed assemblies of Cu^{II} and Cd^{II} coordination polymers with bpt and terephthalate, displaying a unique 3-D polythreading architecture or a 2-fold interpenetrating layered network, have been reported in a latest Communication.[13a] A comprehensive research on the product diversity of coordination architectures with bpt and trimesic acid has also been carried out under different reactive pathways.[13b] Moreover, these results reveal that the mixed-ligand synthetic approach on the basis of bpt and aromatic polycarboxylate is reliable to achieve unusual metal−organic frameworks. As a continuation of this attractive project, we extend the building blocks from the linear terephthalate to its bent isomers and expect to explore the isomeric effect on network assembly. In this context, we will describe a series of Co^{II}, Ni^{II}, Cu^{II}, Zn^{II}, and Cd^{II} coordination polymers with diverse network structures, which are remarkably manipulated by the isomeric tectons and the metal centers. Solid-state properties for these crystalline materials, such as thermal stability, fluorescent emission, and desorption/adsorption of guest solvents have also been investigated.

(4) (a) Beitone, L.; Huguenard, C.; Gansmuller, A.; Henry, M.; Taulelle, F.; Loiseau, T.; Férey, G. *J. Am. Chem. Soc.* **2003**, *125*, 9102. (b) Roesky, H. W.; Andruh, M. *Coord. Chem. Rev.* **2003**, *236*, 91. (c) Barnett, S. A.; Champness, N. R. *Coord. Chem. Rev.* **2003**, *246*, 145. (d) Batten, S. R. *J. Solid State Chem*. **2005**, *178*, 2475. (e) Pan, L.; Olson, D. H.; Ciemnolonski, L. R.; Heddy, R.; Li, J. *Angew. Chem., Int. Ed*. **2006**, *45*, 616. (f) Robin, A. Y.; Fromm, K. M. *Coord. Chem. Rev.* **2006**, *250*, 2127.

(5) (a) Wang, X.-L.; Qin, C.; Wang, E.-B.; Xu, L.; Su, Z.-M.; Hu, C.-W. *Angew. Chem., Int. Ed.* **2004**, *43*, 5036. (b) Ye, B.-H.; Tong, M.-L.; Chen, X.-M. *Coord. Chem. Rev.* **2005**, *249*, 545. (c) Zhang, Z.-H.; Okamura, T.; Hasegawa, Y.; Kawaguchi, H.; Kong, L.-Y.; Sun, W.-Y.; Ueyama, N. *Inorg. Chem.* **2005**, *44*, 6219.

(6) (a) Kitagawa, S.; Kawata, S. *Coord. Chem. Rev*. **2002**, *224*, 11. (b) Oh, M.; Carpenter, G. B.; Sweigart, D. A. *Acc. Chem. Res*. **2004**, *37*, 1. (c) Fang, Q.-R.; Zhu, G.-S.; Jin, Z.; Xue, M.; Wei, X.; Wang, D.-J.; Qiu, S.-L. *Angew. Chem., Int. Ed.* **2006**, *45*, 6126. (d) Kim, H.; Chun, H.; Kim, G. H.; Lee, H. S.; Kim, K. *Chem. Commun.* **2006**, 2759. (e) *Frontiers in Crystal Engineering*; Tiekink, E., Vittal, J. J., Eds.; John-Wiley & Sons Ltd.: New York, 2006.

(7) (a) Chen, X.-M.; Liu, G.-F. *Chem.−Eur. J.* **2002**, *8*, 4811. (b) Shi, X.; Zhu, G.-S.; Wang, X.-H.; Li, G.-H.; Fang, Q.-R.; Zhao, X.-J.; Wu, G.; Tian, G.; Xue, M.; Wang, R.-W.; Qiu, S.-L. *Cryst. Growth Des.* **2005**, *5*, 341. (c) Xiao, D.-R.; Wang, E.-B.; An, H.-Y.; Su, Z.-M.; Li, Y.-G.; Gao, L.; Sun, C.-Y.; Xu, L. *Chem.−Eur. J.* **2005**, *11*, 6673. (d) Kesanli, B.; Cui, Y.; Smith, M. R.; Bittner, E. W.; Bockrath, B. C.; Lin, W. *Angew. Chem., Int. Ed.* **2005**, *44*, 72. (e) Daiguebonne, C.; Kerbellec, N.; Bernot, K.; Gérault, Y.; Deluzet, A.; Guillou, O. *Inorg. Chem.* **2006**, *45*, 5399.

(8) (a) Vodak, D. T.; Braun, M. E.; Kim, J.; Eddaoudi, M.; Yaghi, O. M. *Chem. Commun.* **2001**, 2534. (b) Tao, J.; Zhang, Y.; Tong, M.-L.; Chen, X.-M.; Yuen, T.; Lin, C.-L.; Huang, X.-Y.; Li, J. *Chem. Commun.* **2002**, 1342. (c) Li, Y.-G.; Hao, N.; Lu, Y.; Wang, E.-B.; Kang, Z.-H.; Hu, C.-W. *Inorg. Chem.* **2003**, *42*, 3119.

(9) (a) Prior, T. J.; Rosseinsky, M. J. *Chem. Commun.* **2001**, 1222. (b) Dai, J.-C.; Wu, X.-T.; Fu, Z.-Y.; Cui, C.-P.; Hu, S.-M.; Du, W.-X.; Wu, L.-M.; Zhang, H.-H.; Sun, R.-Q. *Inorg. Chem.* **2002**, *41*, 1391. (c) Sun, D.-F.; Cao, R.; Weng, J.-B.; Hong, M.-C.; Liang, Y.-C. *J. Chem. Soc., Dalton Trans.* **2002**, 291. (d) Prior, T. J.; Bradshaw, D.; Teat, S. J.; Rosseinsky, M. J. *Chem. Commun*. **2003**, 500. (e) Sun, D.-F.; Cao, R.; Sun, Y.-Q.; Bi, W.-H.; Li, X.-J.; Wang, Y.-Q.; Shi, Q.; Li, X. *Inorg. Chem.* **2003**, *42*, 7512. (f) Almeida Paz, F. A.; Klinowski, J. *Inorg. Chem.* **2004**, *43*, 3948. (g) Lin, Z.-Z.; Jiang, F.-L.; Chen, L.; Yuan, D.-Q.; Hong, M.-C. *Inorg. Chem.* **2005**, *44*, 73.

(10) (a) Pan, L.; Huang, X.-Y.; Li, J.; Wu, Y.-G.; Zheng, N.-W. *Angew. Chem., Int. Ed.* **2000**, *39*, 527. (b) Pan, L.; Frydel, T.; Sander, M. B.; Huang, X. Y.; Li, J. *Inorg. Chem.* **2001**, *40*, 1271. (c) Du, M.; Bu, X.-H.; Guo, Y.-M.; Ribas, J.; Diaz, C. *Chem. Commun.* **2002**, 2550. (d) Zheng, Y.-Z.; Tong, M.-L.; Chen, X.-M. *New J. Chem.* **2004**, *28*, 1412.

(11) (a) Zhang, H.-X.; Kang, B.-S.; Xu, A.-W.; Chen, Z.-N.; Zhou, Z.-Y.; Chan, A. S. C.; Yu, K.-B.; Ren, C. *J. Chem. Soc., Dalton Trans.* **2001**, 2559. (b) Ma, C.-B.; Chen, C.-N.; Liu, Q.-T.; Liao, D.-Z.; Li, L.-C.; Sun, L.-C. *New J. Chem*. **2003**, *27*, 890.

(12) (a) Hennigar, T. L.; MacQuarrie, D. C.; Losier, P.; Rogers, R. D.; Zaworotko, M. J. *Angew. Chem., Int. Ed. Engl.* **1997**, *36*, 972. (b) Brandys, M. C.; Puddephatt, R. J. *Chem. Commun.* **2001**, 1508. (c) Pschirer, N. G.; Curtin, D. M.; Smith, M. D.; Bunz, U. H. F.; zur Loye, H.-C. *Angew. Chem., Int. Ed.* **2002**, *41*, 583. (d) Shin, D. M.; Lee, I. S.; Chung, Y. K. *Inorg. Chem.* **2003**, *42*, 8838. (e) Du, M.; Guo, Y.-M.; Chen, S.-T.; Bu, X.-H.; Batten, S. R.; Ribas, J.; Kitagawa, S. *Inorg. Chem.* **2004**, *43*, 1287. (f) Wenger, O. S.; Henling, L. M.; Day, M. W.; Winkler, J. R.; Gray, H. B. *Inorg. Chem.* **2004**, *43*, 2043. (g) Almeida, F. A.; Klinowski, P. J. *Inorg. Chem.* **2004**, *43*, 3948.

(13) (a) Du, M.; Jiang, X.-J.; Zhao, X.-J. *Chem. Commun.* **2005**, 5521. (b) Du, M.; Jiang, X.-J.; Zhao, X.-J. *Inorg. Chem.* **2006**, *45*, 3998.

Table 1. Crystallographic Data and Structure Refinement Summary

param	1	2	3	4	5	6	9
empirical formula	$C_{20}H_{18}CoN_6O_6$	$C_{20}H_{18}CdN_6O_6$	$C_{20}H_{20}CoN_6O_7$	$C_{29}H_{41}NiN_9O_{10}$	$C_{46}H_{42}Zn_2N_{14}O_{10}$	$C_{28}H_{38}Cd_2N_6O_{18}$	$C_{49}H_{51}Cd_2N_{15}O_{12}$
fw	497.33	550.80	515.35	734.42	1081.68	971.44	1266.85
cryst size/mm^3	0.20 × 0.12 × 0.06	0.32 × 0.18 × 0.20	0.42 × 0.21 × 0.20	0.42 × 0.32 × 0.10	0.32 × 0.20 × 0.12	0.32 × 0.26 × 0.20	0.32 × 0.24 × 0.14
cryst system	monoclinic	monoclinic	triclinic	monoclinic	monoclinic	monoclinic	triclinic
space group	$P2_1/n$	$P2_1/n$	$P\bar{1}$	$P2_1/c$	$P2_1/n$	$C2/c$	$P\bar{1}$
a/Å	14.842(9)	15.149(1)	8.589(2)	10.105(4)	19.813(6)	15.7640(9)	10.981(1)
b/Å	8.535(5)	8.7777(6)	10.096(2)	28.75(1)	10.013(3)	12.8408(7)	11.584(1)
c/Å	16.10(1)	15.912(1)	13.979(3)	13.072(5)	23.062(7)	37.833(2)	22.240(2)
α/deg	90	90	81.271(2)	90	90	90	81.630(1)
β/deg	101.345(9)	102.533(1)	78.165(2)	111.813(6)	92.469(4)	93.358(1)	84.578(1)
γ/deg	90	90	78.788(2)	90	90	90	72.513(1)
V/Å^3	2000(2)	2065.4(3)	1155.9(4)	3525(2)	4571(3)	7645.1(7)	2665.6(4)
Z	4	4	2	4	4	8	2
D_{calc}/g·cm^{-3}	1.652	1.771	1.481	1.384	1.572	1.688	1.578
μ/mm^{-1}	0.913	1.110	0.796	0.616	1.127	1.194	0.873
F(000)	1020	1104	530	1544	2224	3904	1284
tot./indpndt reflcns	10 461/3516	10 868/3648	6293/4013	18 413/6047	24 098/8028	20 317/6718	14 631/9317
R_{int}	0.0667	0.0243	0.0215	0.0787	0.0316	0.0231	0.0239
no. of params	298	298	325	447	653	591	709
R, R_w	0.0483, 0.1078	0.0362, 0.0891	0.0414, 0.1301	0.0584, 0.1216	0.0380, 0.0928	0.0393, 0.1093	0.0338, 0.0753
goodness-of-fit	1.057	1.084	1.075	1.024	1.015	1.087	1.002
resids (e Å^{-3})	0.377, −0.499	1.852, −0.888	0.633, −0.408	1.050, −0.590	0.935, −0.574	0.884, −0.638	0.492, −0.525

Experimental Section

General Materials and Methods. With the exception of the ligand bpt, which was prepared according to the literature procedure,[14] all reagents and solvents for synthesis and analysis were commercially available and used as received. Elemental analyses were performed on a CE-440 (Leemanlabs) analyzer. Fourier transform (FT) IR spectra (KBr pellets) were taken on an AVATAR-370 (Nicolet) spectrometer. Thermogravimetric analysis (TGA) experiments were carried out on a Dupont thermal analyzer from room temperature to 800 °C under nitrogen atmosphere at a heating rate of 10 °C/min. Solid-state fluorescence spectra were recorded on a Cary Eclipse spectrofluorometer (Varian) equipped with a xenon lamp and quartz carrier at room temperature. X-ray powder diffraction (XRPD) patterns were taken on a Rigaku RU200 diffractometer for Cu Kα radiation (λ = 1.5406 Å), with a scan speed of 2 °/min and a step size of 0.02° in 2θ. The calculated XRPD patterns were produced from single-crystal X-ray reflection data.

Syntheses of the Complexes. {**[Co(bpt)(pa)(H$_2$O)]·H$_2$O**}$_n$ **(1).** A mixture containing $Co(OAc)_2·4H_2O$ (30.0 mg, 0.12 mmol), bpt (24.0 mg, 0.10 mmol), H_2pa (16.6 mg, 0.10 mmol), and water (10 mL) was sealed in a Teflon-lined stainless steel vessel (20 mL), which was heated at 140 °C for 3 days and then cooled to room temperature at a rate of 5 °C/h. Red prism crystals of **1** were collected in a 60% yield (30.0 mg, based on bpt). Anal. Calcd for $C_{20}H_{18}CoN_6O_6$: C, 48.30; H, 3.65; N, 16.90. Found: C, 48.65; H, 3.62; N, 16.85. IR (cm^{-1}): 3346 s, 3265 s, 1663 w, 1609 vs, 1551 vs, 1486 s, 1462 s, 1406 vs, 1378 vs, 1229 m, 1065 w, 999 m, 956 w, 839 m, 771 m, 741 m, 700 s, 605 s, 507 m.

{**[Cd(bpt)(pa)(H$_2$O)]·H$_2$O**}$_n$ **(2).** The same synthetic procedure as that for **1** was used except that $Co(OAc)_2·4H_2O$ was replaced by $Cd(OAc)_2·2H_2O$, giving colorless block X-ray-quality crystals in a 57% yield (31.2 mg). Anal. Calcd for $C_{20}H_{18}CdN_6O_6$: C, 43.61; H, 3.29; N, 15.26. Found: C, 44.04; H, 3.74; N, 15.68. IR (cm^{-1}): 3344 s, 3272 s, 1610 s, 1553 vs, 1455 s, 1384 vs, 1229 m, 997 m, 955 w, 839 m, 772 m, 739 m, 699 s, 605 m, 504 w.

{**[Co(bpt)(ip)]·3H$_2$O**}$_n$ **(3).** The same synthetic procedure as that for **1** was used except that H_2pa was replaced by H_2ip, yielding pink prism X-ray-quality crystals of **3** in a 70% yield (36.0 mg). Anal. Calcd for $C_{20}H_{20}CoN_6O_7$: C, 46.61, H, 3.91; N, 16.31. Found: C, 47.06; H, 3.55; N, 16.43. IR (cm^{-1}): 3332 bs, 1615 vs, 1581 m, 1544 s, 1456 s, 1399 vs, 1220 m, 1106 w, 917 w, 836 s, 740 s, 720 s, 615 m, 521 m, 433 m.

{**[Ni(bpt)(ip)(H$_2$O)]·2H$_2$O·3DMF**}$_n$ **(4).** A hot EtOH (30 mL) solution of bpt (24.0 mg, 0.10 mmol) was mixed with an aqua solution (5 mL) of $Ni(OAc)_2·4H_2O$ (27.0 mg, 0.11 mmol) with stirring. Then a solution of H_2ip (17.0 mg, 0.10 mmol) in DMF (5 mL) was added to above mixture with continuous stirring for about 30 min. The filtrate was left to stand at room temperature. Green block crystals suitable for X-ray analysis were produced by slow evaporation of the solvents after a period of 2 weeks in a 40% yield (29.0 mg, based on bpt). Anal. Calcd for $C_{29}H_{41}NiN_9O_{10}$: C, 47.43; H, 5.63; N, 17.17. Found: C, 47.32; H, 5.52; N, 17.15. IR (cm^{-1}): 3300 bs, 3163 bs, 1669 vs, 1609 vs, 1548 vs, 1440 s, 1379 vs, 1255 w, 1222 m, 1100 m, 1068 w, 985 w, 842 m, 746 s, 708 s, 663 m, 608 m, 514 w.

{**[Zn(bpt)(ip)]$_2$·2DMF**}$_n$ **(5).** The same synthetic procedure as that for **4** was used except that $Ni(OAc)_2·4H_2O$ was replaced by $Zn(OAc)_2·2H_2O$, producing colorless block crystals of **5** in a 25% yield (13.4 mg). Anal. Calcd for $C_{46}H_{42}Zn_2N_{14}O_{10}$: C, 51.08; H, 3.91; N, 18.13. Found: C, 51.24; H, 3.54; N, 18.59. IR (cm^{-1}): 3328 bs, 3058 m, 1674 s, 1615 vs, 1549 s, 1449 s, 1392 vs, 1220 m, 1017 w, 982 w, 837 m, 742 s, 721 s, 612 m, 518 m.

{**[Cd$_2$(bpt)(ip)$_2$(H$_2$O)$_4$]·6H$_2$O**}$_n$ **(6).** The same synthetic procedure as that for **1** was used except that $Co(OAc)_2·4H_2O$ and H_2pa were replaced by $Cd(OAc)_2·2H_2O$ and H_2ip, respectively. Colorless block crystals of **6** were collected in a 75% yield (36.5 mg, based on H_2ip). Anal. Calcd for $C_{28}H_{38}Cd_2N_6O_{18}$: C, 34.62; H, 3.94; N, 8.65. Found: C, 34.95; H, 3.66; N, 8.98. IR (cm^{-1}): 3443 bs, 3303 s, 1608 vs, 1558 s, 1443 s, 1389 vs, 1221 m, 1070 w, 980 w, 935 w, 831 s, 727 s, 662 m, 606 m, 510 m.

{**[Cu(bpt)(tp)(H$_2$O)]$_2$[Cu(bpt)$_2$(tp)](H$_2$O)$_2$**}$_n$ **(7)** and {**[Cd(bpt)-(tp)(H$_2$O)]$_2$(DMF)$_{1.5}$(H$_2$O)**}$_n$ **(8).** A synthetic procedure similar to that for **4** was used. See ref 13a for details of preparation and characterization of both complexes.

{**[Cd$_2$(bpt)$_2$(tp)$_2$(H$_2$O)(DMF)]·2DMF**}$_n$ **(9).** The same synthetic method as that for **8** was used except that $Cd(OAc)_2·2H_2O$ was replaced by $Cd(NO_3)_2·4H_2O$. Colorless block crystals of **9** suitable

(14) Bentiss, F.; Lagrenee, M.; Traisnel, M.; Mernari, B.; Elattari, H. *J. Heterocycl. Chem.* **1999**, *36*, 149.

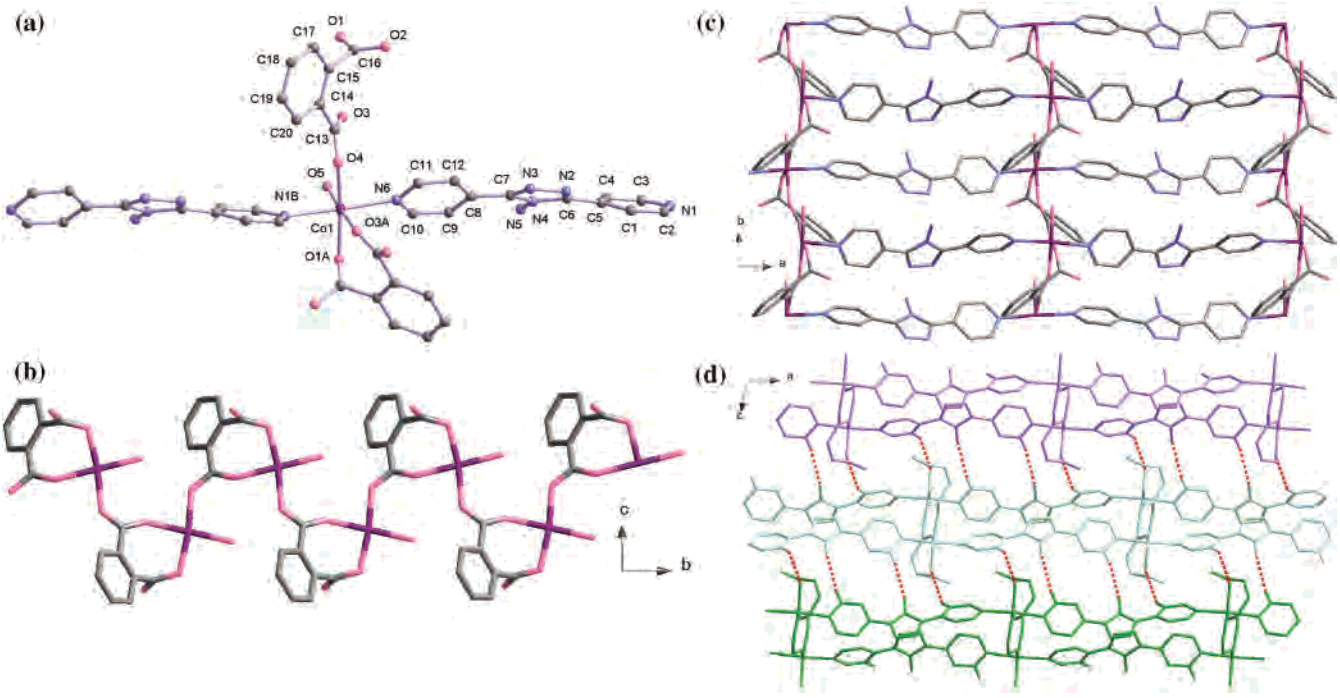

Figure 1. (a) Portional view of **1** with atom labeling of the asymmetric unit and metal coordination. Symmetry codes are listed in Table 2. The lattice water molecule is omitted for clarity. (b) Perspective view of the pa-bridged chain structure. (c) Perspective view of the 2-D layered framework extended along the *ab* plane. (d) 3-D network of **1** showing interlayer hydrogen-bonding interactions.

for X-ray diffraction were collected in a 30% yield (19.1 mg). Anal. Calcd for $C_{49}H_{51}Cd_2N_{15}O_{12}$: C, 46.46; H, 4.06; N, 16.58. Found: C, 45.95; H, 3.40; N, 16.24. IR (cm^{-1}): 3364 bm, 1667 vs, 1611 vs, 1571 vs, 1502 w, 1384 vs, 1223 w, 1096 w, 1007 m, 886 w, 838 m, 748 m, 667 w, 610 w, 516 m.

X-ray Crystallography. Crystallographic details for complexes **7** and **8** have been described in the previous Communication.[13a] X-ray single-crystal diffraction data for **1**−**6** and **9** were collected on a Bruker Apex II CCD diffractometer at room temperature with Mo Kα radiation (λ = 0.710 73 Å). There was no evidence of crystal decay during data collection. A semiempirical absorption correction was applied using SADABS, and the program SAINT was used for integration of the diffraction profiles.[15] The structures were solved by direct methods using SHELXS and refined with SHELXL.[16] The final refinements were performed by full-matrix least-squares methods with anisotropic thermal parameters for all non-H atoms on F^2. Hydrogen atoms bound to carbon and nitrogen were placed geometrically and allowed to ride during the subsequent refinements with isotropic displacement parameters. Generally, starting positions for water H atoms were found in difference syntheses and then fixed in the given positions. For **3**, the H atoms of two lattice water molecules (O8 and O9, modeled with a half-occupancy) were not located. In the structure of **6**, all H atoms associated with the lattice and coordination water molecules were not determined. One pyridyl ring of bpt in **6** was treated using a disordered model, which was divided into two equivalent parts. For **2**, the highest residual electron density peak (1.852 e·Å^{-3}) is associated with the Cd1 center (0.87 Å from Cd1). Further crystallographic data and structural refinement details are summarized in Table 1.

(15) *SAINT Software Reference Manual*; Bruker AXS: Madison, WI, 1998.
(16) Sheldrick, G. M. *SHELXTL NT, Version 5.1. Program for Solution and Refinement of Crystal Structures*; University of Göttingen: Göttingen, Germany, 1997.

Results and Discussion

Preparation of 1−9. Two synthetic approaches were applied to achieve these coordination polymers. With regard to MOFs **1**−**3** and **6**, they were prepared under hydrothermal conditions, whereas assemblies of the others were carried out directly in C_2H_5OH/H_2O/DMF mixed media in general conditions. The phase purities of the bulk samples were confirmed by the X-ray powder diffraction (XRPD) technique (see Figure S1 in the Supporting Information for XRPD patterns). In each synthetic case, an approximate metal/ligand composition of 1:1:1 was utilized for the starting materials. Notably, most of the resultant complexes were also obtained with this equimolar composition, whereas a stoichiometric ratio of 2:1:2 or 3:4:3 (Cd:bpt:ip or Cu:bpt:tp) was found in **6** or **7**. It is of special interest that the utilization of different Cd^{II} sources (acetate vs nitrate) can lead to the formation of two dissimilar crystalline products **8** and **9**, although the inorganic anions are not invlolved in both materials. Coordination polymers **1**−**9** are air stable with the maintenance of their crystallinity for at least several weeks and are insoluble in common organic solvents and water, being consistent with their polymeric and neutral nature.

Structural Analysis and Discussion. {[Co(bpt)(pa)(H$_2$O)]·H$_2$O}$_n$ (1) and {[Cd(bpt)(pa)(H$_2$O)]·H$_2$O}$_n$ (2). X-ray diffraction studies reveal that complexes **1** and **2** are isostructural (see Table 1), and therefore, only the crystal structure of **1** will be described in detail. The asymmetric unit and metal coordination of **1** is shown in Figure 1a. Each Co^{II} center is located in a six-coordinated octahedral environment, being surrounded by a pair of pyridyl nitrogens of bpt, three carboxylate oxygen atoms from pa, and a water ligand

Table 2. Selective Bond Lengths (Å) and Angles (deg) for Complex **1**[a]

Co1−O1A	2.059(3)	Co1−O4	2.074(3)
Co1−O5	2.102(3)	Co1−O3A	2.103(3)
Co1−N6	2.166(3)	Co1−N1B	2.177(3)
O1−C16	1.268(4)	O2−C16	1.231(5)
O3−C13	1.245(4)	O4−C13	1.261(4)
O1A−Co1−O4	170.3(1)	O1A−Co1−O5	88.7(1)
O4−Co1−O5	99.1(1)	O1A−Co1−O3A	90.8(1)
O4−Co1−O3A	81.8(1)	O5−Co1−O3A	176.7(1)
O1A−Co1−N6	94.0(1)	O4−Co1−N6	91.9(1)
O5−Co1−N6	88.6(1)	O3A−Co1−N6	88.2(1)
O1A−Co1−N1B	89.9(1)	O4−Co1−N1B	83.7(1)
O5−Co1−N1B	95.7(1)	O3A−Co1−N1B	87.6(1)
N6−Co1−N1B	174.3(1)		

[a] Symmetry codes: (A) $-x + 1/2, y - 1/2, -z + 1/2$; (B) $x - 1, y, z$.

(see Table 2 for detailed bond parameters). As illustrated in Figure 1b, one carboxylate is monodentate whereas the other adopts a *syn-anti* bridging mode. As a consequence, each Co^{II} ion forms a 7-membered chelated ring with pa, and the adjacent Co^{II} centers are connected by pa components with a separation of 5.263(5) Å to furnish a polymeric chain along the [010] direction. As illustrated in Figure 1c, these 1-D arrays are further interlinked through bpt spacers to generate a 2-D (4,4) coordination layer along the *ab* plane with the Co···Co separation by bpt of 14.842(9) Å. Further investigation of crystal packing reveals that these parallel 2-D arrays are extended via interlayer C4−H4···O1 and C10−H10···N5 interactions (see Table S1 in the Supporting Information for details) along [001] to build a 3-D architecture (see Figure 1d).

The crystal structure of **2** is isomorphic to **1** with only a small difference. As expected, because of the larger ion radius of Cd^{II}, all coordinative bond distances in **2** are significantly longer than those in **1**, as listed in Table S2 (see Supporting Information). Also, the octahedral metal sphere of Cd^{II} displays a more distortion due to the steric effect.

Two related isostructural compounds, namely $[M(bipy)(pa)(H_2O)]_n$ (M = Co^{II} or Cd^{II}; bipy = 4,4′-bipyridine) have been reported,[17] the coordination frameworks of which are similar to those of **1** and **2** except forming less corrugated layers. This should be ascribed to the bent backbone of bpt compared with that of the rodlike bipy molecule. Notably, another greatly different example of $[Co(Hpa)_2(bipy)]_n$ has been hydrothermally prepared.[18] It shows a complicated 3-D array built from the linear Co−bipy chains that are extended by four symmetry-equivalent Hpa anions in different directions, and thus each metal node is surrounded by four Hpa and two bipy to furnish six valid linkages in the network generation.

$\{[Co(bpt)(ip)]\cdot 3H_2O\}_n$ (3). Complex **3** displays an interesting double-layer framework. As depicted in Figure 2a, each distorted octahedral Co^{II} center is defined by four equatorial oxygen donors and two axial nitrogen atoms, coming from three ip and a pair of bpt ligands, respectively

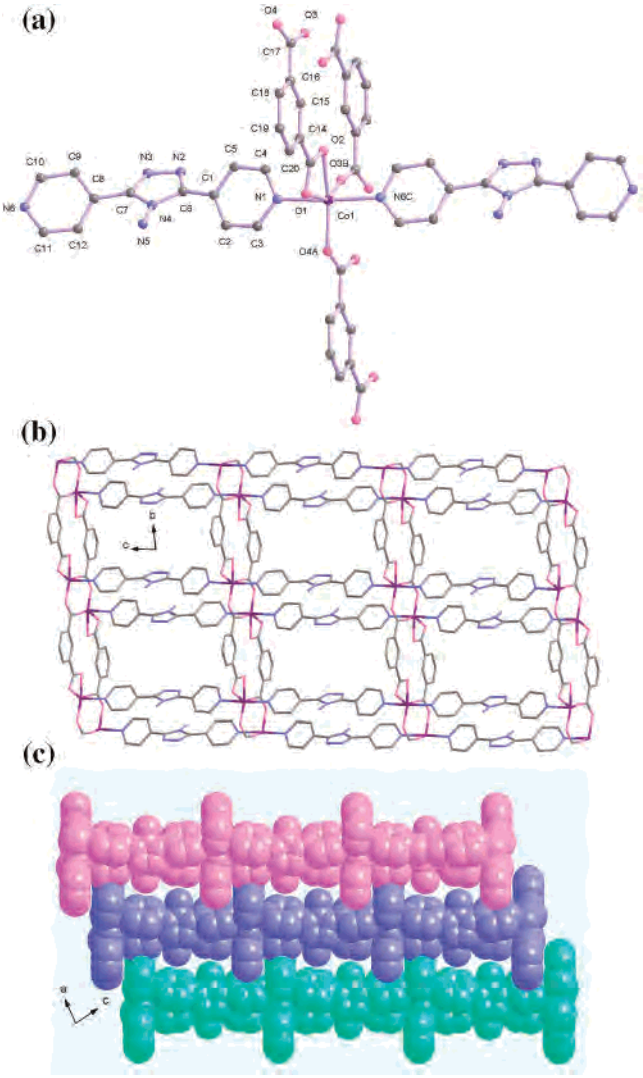

Figure 2. (a) Portional view of **3** with atom labeling of the asymmetric unit and metal coordination. Symmetry codes are listed in Table 3. The lattice water molecules are omitted for clarity. (b) Perspective view of the 2-D double-layered framework of **3**. (c) Packing diagram in the space-filling model showing the interdigitating arrangement of the 2-D arrays in **3**.

Table 3. Selective Bond Lengths (Å) and Angles (deg) for Complex **3**[a]

Co1−O4A	2.021(2)	Co1−O3B	2.028(2)
Co1−O2	2.142(2)	Co1−N1	2.153(3)
Co1−N6C	2.155(3)	Co1−O1	2.254(2)
O1−C13	1.255(4)	O2−C13	1.253(4)
O3−C17	1.243(4)	O4−C17	1.254(4)
O4A−Co1−O3B	116.67(9)	O4A−Co1−O2	152.3(1)
O4A−Co1−N1	91.6(1)	O3−Co1−N1	85.1(1)
O2−Co1−N1	91.9(1)	O3B−Co1−O2	91.02(9)
O3B−Co1−N6C	88.8(1)	N1−Co1−O1	86.8(1)
O2−Co1−N6C	86.4(1)	N1−Co1−N6C	173.6(1)
O4A−Co1−O1	93.23(9)	O3B−Co1−O1	149.17(9)
O2−Co1−O1	59.55(8)	O4A−Co1−N6C	92.8(1)
N6C−Co1−O1	97.5(1)		

[a] Symmetry codes: (A) $x, y - 1, z$; (B) $-x + 1, -y + 2, -z + 1$; (C) $x + 1, y, z - 1$.

(see Table 3 for detailed bond parameters). The two independent carboxylate groups in each ip ligand function as a chelated bidentate and a *syn-syn* bridging, respectively, and thus the metal centers are extended by the ip linkers to result in a 1-D Co^{II}−ip ribbon along [010]. The linkages of

(17) Suresh, E.; Boopalan, K.; Jasra, R. V.; Bhadbhade, M. M. *Inorg. Chem.* **2001**, *40*, 4078.
(18) Lightfoot, P.; Snedden, A. *J. Chem. Soc., Dalton Trans.* **1999**, 3549.

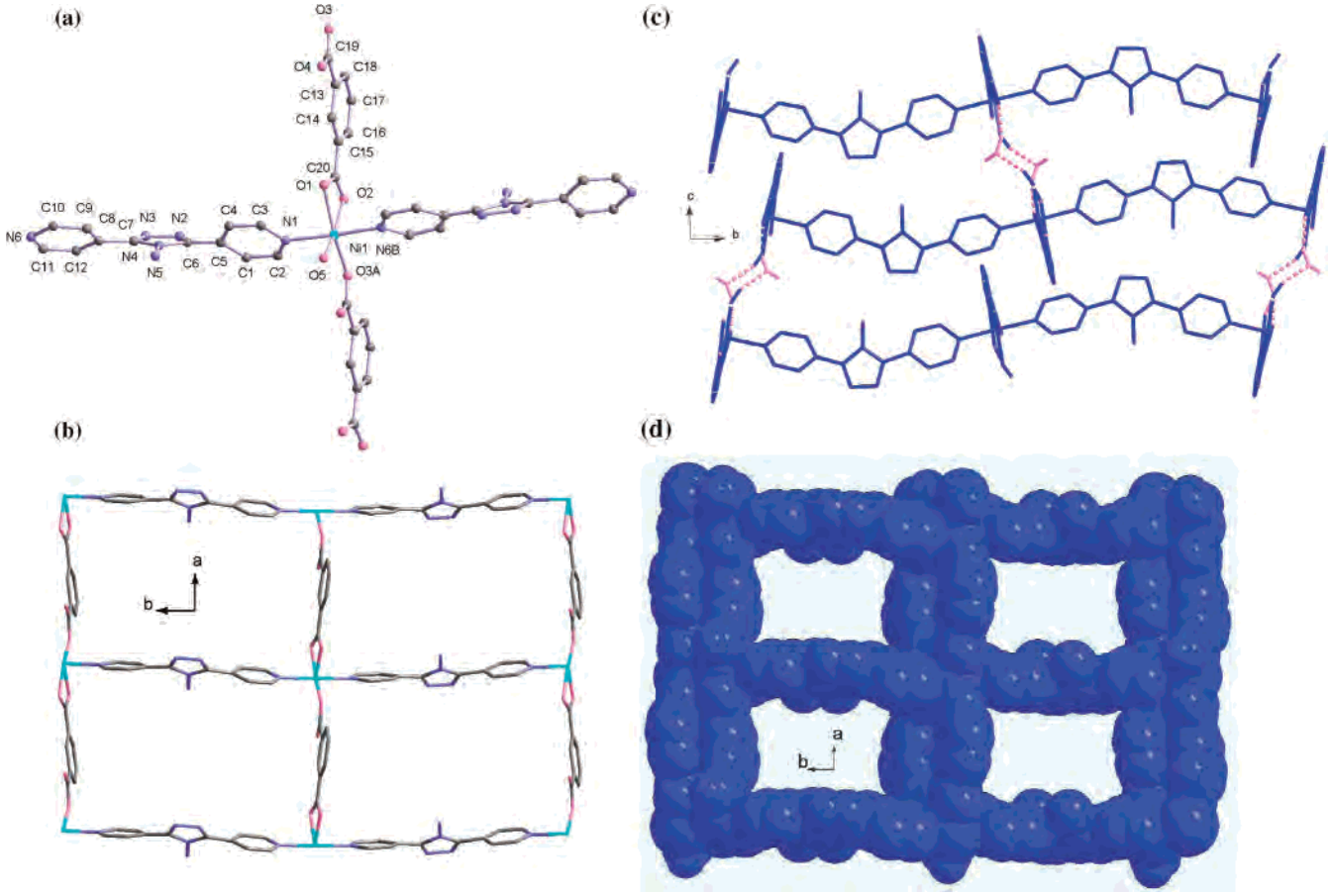

Figure 3. (a) Portional view of **4** with atom labeling of the asymmetric unit and metal coordination. Symmetry codes are listed in Table 4. The lattice solvents are omitted for clarity. (b) 2-D coordination layer of **4**. (c) 3-D network of **4** showing interlayer hydrogen-bonding interactions. (d) Packing diagram of **4** in the space-filling model, showing the rectangular channels along the [001] direction. The accommodated solvents are omitted for clarity.

such ribbons via exo-bidentate bpt ligands along [10$\bar{1}$] further generate a 2-D double-layer motif (see Figure 2b). A more revealing description from the viewpoint of network topology is that the adjacent dinuclear Co^{II} nodes are extended along the (101) plane via four paired ip and bpt connectors to form a 2-D (4,4) network. The Co···Co distance separated by the bpt linker is 14.83(2) Å, and it is 4.194(3) Å in the dimeric unit bridged by a pair of carboxylate groups. A side view from the [010] direction indicates that the ip entities are located at both sides of each 2-D framework, and as a consequence, such parallel arrays are interdigitated with the presence of significant interlayer aromatic stacking between the ip ligands (see Figure 2c). The centroid-to-centroid and centroid-to-face separations of the neighboring phenyl rings are ca. 3.72 and 3.46 Å, respectively.

{[Ni(bpt)(ip)(H_2O)]·2H_2O·3DMF}$_n$ (4). Complex **4** features a simple 2-D layered network in which the metal centers are interlinked by ip and bpt bridges. As shown in Figure 3a, each Ni^{II} atom is surrounded by four oxygen donors from two ip and a water ligand in the basal plane and two pyridyl nitrogen atoms from a pair of bpt in trans-arrangement at the apical sites, displaying a distorted octahedral geometry (see Table 4 for detailed bond parameters). In this structure, the carboxylate groups of ip behave in monodentate and chelated bidentate fashions, respectively. The Ni^{II} centers are propagated along the *ab* plane via bridged spacers of ip and bpt to result in a 2-D sheet with dimensions of 10.105(4) × 14.406(6) $Å^2$ (see Figure 3b). These 2-D sheets are parallel and further extended to a 3-D network via O5−H5A···O9 and O9−H9A···O1 interactions (see Table S1 for details) between the lattice and coordination aqua molecules (see Figure 3c). As a matter of fact, this 3-D host architecture is porous. As shown in Figure 3d, 1-D rectangle channels are observed along the [001] direction, possessing a void volume of 1199 $Å^3$ (34%)/unit cell, which are occupied by the lattice solvents such as water and DMF. Beyond this, multiple hydrogen-bonding contacts between the 3-D host and solvent guests are also detected to further sustain this structure. As

Table 4. Selective Bond Lengths (Å) and Angles (deg) for Complex **4**[a]

Ni1−O3A	2.003(4)	Ni1−O5	2.042(4)
Ni1−N6B	2.089(4)	Ni1−N1	2.102(4)
Ni1−O2	2.119(4)	Ni1−O1	2.129(4)
O1−C20	1.271(6)	O2−C20	1.245(6)
O3−C19	1.263(6)	O4−C19	1.220(7)
O3A−Ni1−O5	96.4(2)	O3A−Ni1−N6B	92.4(2)
O5−Ni1−N6B	87.2(2)	O3A−Ni1−N1	91.0(2)
O5−Ni1−N1	92.5(2)	N6B−Ni1−N1	176.6(2)
O3A−Ni1−O2	99.8(1)	O5−Ni1−O2	163.4(1)
N6B−Ni1−O2	88.4(2)	N1−Ni1−O2	91.0(2)
O3A−Ni1−O1	161.9(2)	O5−Ni1−O1	101.6(2)
N6B−Ni1−O1	87.8(2)	N1−Ni1−O1	88.9(2)
O2−Ni1−O1	62.2(1)		

[a] Symmetry codes: (A) $x + 1, y, z$; (B) $-x + 2, y + 1/2, -z + 3/2$.

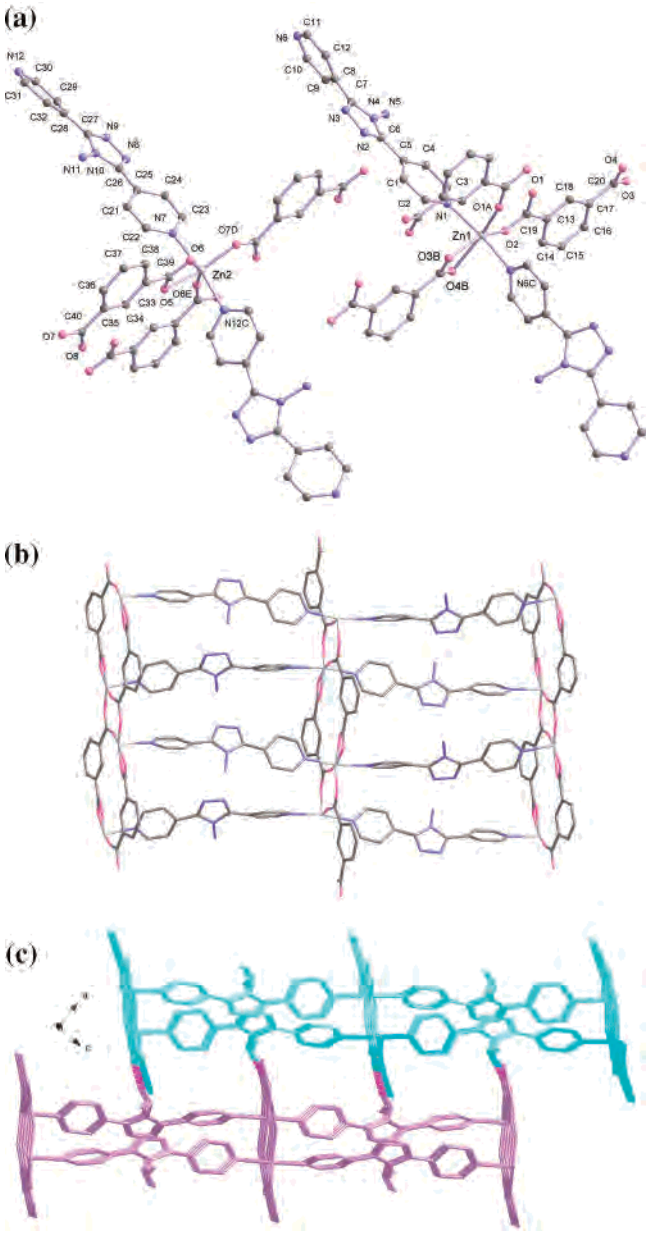

Figure 4. (a) Portional view of **5** with atom labeling of the asymmetric unit and metal coordination. Symmetry codes are listed in Table 5. The lattice DMF molecules are omitted for clarity. (b) 2-D coordination framework of **5**. (c) 3-D network of **5** showing interlayer hydrogen bonds.

for $[Ni(ip)(bipy)]_n$,[19] it displays a 2-D double-layer network similar to that of $\{[Co(bpt)(ip)]\cdot 3H_2O\}_n$ (**3**). This structural discrepancy may arise from the different coordination modes of ip with Ni^{II} ions in both cases.

$\{[Zn(bpt)(ip)]_2\cdot 2DMF\}_n$ (5). Complex **5** also shows a 2-D layered network, in which two similar crystallographically independent [Zn(bpt)(ip)] fragments are observed, as depicted in Figure 4a. Each Zn^{II} center is in a distorted octahedral geometry (see Table 5 for detailed bond parameters), being completed by two trans-related bpt molecules at the axial positions and four oxygen atoms from three separated ip ligands in the equatorial plane. The two distinct carboxylate groups in each complex unit adopt the chelating bidentate and *syn-anti* bridging coordination fashions, respectively. Thus, two adjacent Zn1 (or Zn2) atoms are bridged by a pair of *syn-anti* carboxylates to form a dinuclear unit, within which the Zn···Zn separation is 4.468(3) Å (4.432(3) Å for Zn2). Along the [010] direction, these dimeric subunits are extended by a pair of ip ligands to afford 1-D ribbons, and interlinks of such ribbons through the exo-bidentate bpt entities further furnish an infinite 2-D framework (see Figure 4b). In addition, these parallel 2-D coordination layers are staggered and interlinked via N5···H5A O6 and N11···H11A O3 interactions (see Table S1 for details) to finally produce a 3-D supramolecular architecture, as shown in Figure 4c.

Apparently, this layered coordination structure is similar to that of MOF **3**. In fact, the simplified layers in both cases are 3,5-connected nets with the metal ions as 5-connected and the ip anions as 3-connected nodes (each bpt is just a 2-connecting spacer). If the dimeric SBUs (secondary building units) are considered as nodes, thus, both layered networks in **3** and **5** become uninodal, in which eight ligands (four bpt and four ip) depart from each SBU. However, a careful analysis reveals that the same nodes are linked to each other differently in the networks of **3** and **5** (see Scheme S1 in the Supporting Information). In the case of **3**, each SBU is linked to only four other SBUs with all the connections of bpt and ip as double bridges to build a decorated (4,4) layer (sql[20] net). However, in the structure of **5**, the bpt bridges are no more acting in pairs between the SBUs but as single connectors. As a result, the overall connectivity is increased to six in this case and the resultant framework is properly described as a decorated (3,6) layer

Table 5. Selective Bond Lengths (Å) and Angles (deg) for Complex **5**[a]

Zn1−O2	2.001(2)	Zn1−O1A	2.058(2)
Zn1−N1	2.182(2)	Zn1−N6C	2.201(3)
Zn1−O4B	2.125(2)	Zn1−O3B	2.370(2)
O1−C19	1.239(3)	O2−C19	1.269(3)
O3−C20	1.252(3)	O4−C20	1.263(3)
Zn2−O5	2.083(2)	Zn2−N7	2.203(2)
Zn2−O6	2.364(2)	Zn2−O7D	1.992(2)
Zn2−O8E	2.055(2)	Zn2−N12C	2.188(3)
O5−C39	1.262(3)	O6−C39	1.246(3)
O7−C40	1.264(3)	O8−C40	1.244(3)
O2−Zn1−O1A	108.04(8)	O2−Zn1−O4B	147.81(8)
O1A−Zn1−O4B	103.77(8)	O2−Zn1−N1	97.87(9)
O1A−Zn1−N1	91.13(9)	O4B−Zn1−N1	86.17(9)
O2−Zn1−N6C	91.68(9)	O1A−Zn1−N6C	89.18(9)
O4B−Zn1−N6C	83.90(8)	N1−Zn1−N6C	169.84(9)
O2−Zn1−O3B	89.83(8)	O1A−Zn1−O3B	162.08(8)
O4B−Zn1−O3B	58.31(7)	N1−Zn1−O3B	87.60(9)
N6C−Zn1−O3B	88.99(9)	O7D−Zn2−O8E	108.33(8)
O7D−Zn2−O5	149.18(8)	O8E−Zn2−O5	102.44(8)
O7D−Zn2−N12C	94.82(9)	O8E−Zn2−N12C	93.6(1)
O5−Zn2−N12C	84.89(8)	O7D−Zn2−N7	91.75(9)
O8E−Zn2−N7	86.1(1)	O5−Zn2−O7D	88.47(8)
N12C−Zn2−N7	173.15(9)	O7D−Zn2−O6	90.53(8)
O8E−Zn2−O6	160.84(8)	O5−Zn2−O6	58.65(7)
N12C−Zn2−O6	87.96(9)	N7−Zn2−O6	90.04(9)

[a] Symmetry codes: (A) $-x+2, -y+1, -z+2$; (B) $x, y+1, z$; (C) $x+1/2, -y+3/2, z+1/2$; (D) $x, y-1, z$; (E) $-x+1, -y+2, -z+2$.

(19) Tao, J.; Chen, X.-M.; Huang, R.-B.; Zheng, L.-S. *J. Solid State Chem.* **2003**, *170*, 130.

(20) For the three-letter net codes, see the website of Reticular Chemistry Structure Resource (RCSR): http://okeeffe-ws1.la.asu.edu/RCSR/home.htm.

(hxl[20] net). Notably, such a network topology is quite unusual in comparison with that of the pertinent 2-D 3-connected (6,3) layer, which is commonly observed for MOFs.[21]

A quite different example is $[Zn_4O(ip)_3(bipy)]_n$,[22] in which the central μ_4-oxo atoms link the zinc ions to form Zn_4O cores, which are further connected by bipy bridges to generate a 2-D framework with two types of cavities. Two other related Zn^{II} coordination polymers, namely, $\{[Zn(ip)(bipy)(H_2O)]\cdot 1.5H_2O\}_n$ and $\{[Zn_2(ip)_2(bipy)(EtOH)(H_2O)_2]\cdot EtOH\cdot 0.5H_2O\}_n$,[23] have been obtained using the diffusion method. They are prepared under different proportions of the starting materials, which give rise to the acidity discrepancy of the reactive solutions and thus lead to the formation of two distinct products. The former has a 2-D layered network with approximately square units, whereas the latter features an interpenetrating 2-D herringbone-like structure.

$\{[Cd_2(bpt)(ip)_2(H_2O)_4]\cdot 6H_2O\}_n$ (6). The structure of **6** displays an interesting alternately interpenetrated and interdigitated architecture on the basis of the T-shaped bilayer motifs. The fundamental building unit (see Figure 5a) contains two independent Cd^{II} centers, two pairs of symmetry-related ip, four water ligands, and a bpt spacer (see Table 6 for detailed bond parameters). The Cd1 ion adopts a distorted pentagonal-dipyramidal geometry via coordinating to one nitrogen of bpt and four oxygens of two ip dianions in the equatorial plane and two water molecules at the axial sites with the O−Cd−O angle of 175.1(2)°. However, the octahedral Cd2 center is provided by one nitrogen atom from bpt, as well as five oxygen atoms from two ip dianions and a pair of water ligands. Furthermore, Cd2 is weakly bonded to O7 with the Cd−O distance of 2.796(5) Å. In the network structure of **6**, each Cd^{II} ion behaves as a three-connected T-shaped coordination configuration, with the carboxylate oxygen donors of a pair of ip dianions in the horizontal orientations and a pyridyl nitrogen donor of bpt in the vertical direction. As a consequence, the extension of such T-shaped Cd^{II} nodes results in the formation of a 2-D bilayer motif with $8^2.10$ network topology, as illustrated in Figure 5b. This topology is uncommon in comparison with the other coordination frameworks based on the T-shaped nodes, such as the types of 1-D ladder, 2-D brick wall, and 3-D network.[24] Of further interest, the bilayer arrays in **6** display a unique structural feature of 3-D packing, which are alternately interpenetrating and interdigitating. As depicted in Figure 5b, two adjacent bilayer arrays with the same orientation (highlighted as magenta and blue) are interpenetrated in a parallel fashion. Also, the pairs of such opposite "double bilayers" are interdigitated in a "tongue-and-groove" stacking mode (see Figure 5c). In addition, the final 3-D crystalline lattice is reinforced through the significant aromatic stacking between the benzene and triazole rings in the "tongue"

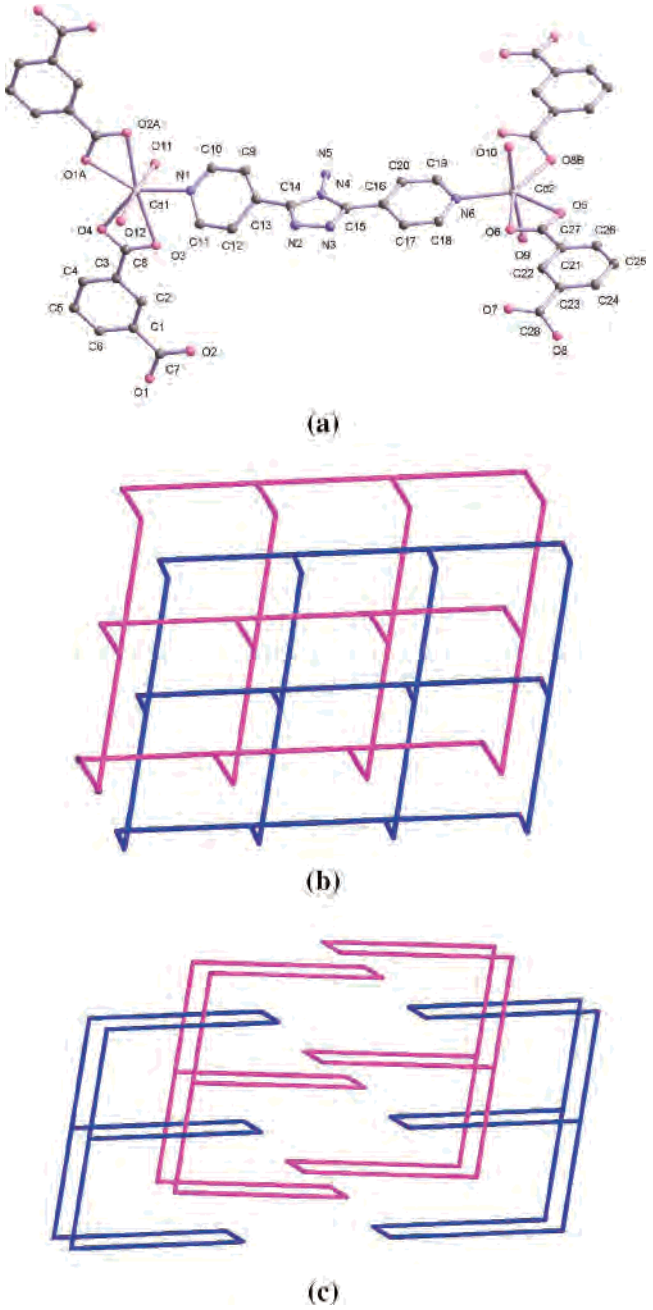

Figure 5. (a) Portional view of **6** with atom labeling of the asymmetric unit and metal coordination. Symmetry codes are listed in Table 6. The lattice water molecules are omitted for clarity. (b) Schematic representation of the interpenetrating bilayer motifs with $8^2.10$ topology. (c) Schematic representation showing the alternately interpenetrated and interdigitated architecture of the bilayer motifs in **6**. The ip and bpt linkers are simplified as rods for clarity.

sections, with the centroid-to-centroid and centroid-to-face distances of ca. 3.45 and 3.34/3.37 Å, respectively. Notably, a related compound $\{[Cd(ip)(bipy)]\cdot H_2O\}_n$[19] is obtained under similar hydrothermal conditions, which however shows a 2-D double-layer network homologous to that of $[Ni(ip)(bipy)]_n$ as stated above.

$\{[Cu(bpt)(tp)(H_2O)]_2[Cu(bpt)_2(tp)](H_2O)_2\}_n$ (7). The supramolecular organization of **7** is unexpected and consists of two types of coordination frameworks. One is a 1-D tp-bridged chain with the monodentate bpt segments as the side arms, whereas the other has a simple 2-D (4,4) plane

(21) Su, C.-Y.; Cai, Y.-P.; Chen, C.-L.; Kang, B.-S. *Inorg. Chem.* **2001**, *40*, 2210.
(22) Tao, J.; Tong, M.-L.; Shi, J.-X.; Chen, X.-M.; Ng, S. W. *Chem. Commun.* **2000**, 2043.
(23) Xu, L.; Guo, G.-C.; Liu, B.; Wang, M.-S.; Huang, J.-S. *Inorg. Chem. Commun.* **2004**, *7*, 1145.
(24) (a) Du, M.; Zhao, X.-J. *Inorg. Chem. Commun.* **2004**, *7*, 1056. (b) Biradha, K.; Sarkar, M.; Rajput, L. *Chem. Commun.* **2006**, 4169 and references therein.

Table 6. Selective Bond Lengths (Å) and Angles (deg) for Complex **6**[a]

Cd1−N1	2.281(4)	Cd1−O1A	2.293(3)
Cd1−O4	2.319(3)	Cd1−O12	2.329(4)
Cd1−O11	2.329(4)	Cd1−O3	2.535(3)
Cd1−O2A	2.573(3)	Cd2−O8B	2.236(4)
Cd2−N6	2.266(4)	Cd2−O5	2.319(4)
Cd2−O9	2.362(4)	Cd2−O10	2.408(4)
Cd2−O6	2.476(4)	O1−C7	1.277(6)
O2−C7	1.244(6)	O3−C8	1.242(6)
O4−C8	1.267(5)	O5−C27	1.269(7)
O6−C27	1.246(7)	O7−C28	1.233(6)
O8−C28	1.265(6)		
N1−Cd1−O1A	140.6(1)	N1−Cd1−O4	136.1(1)
O1A−Cd1−O4	82.2(1)	N1−Cd1−O12	85.2(2)
O1A−Cd1−O12	89.6(2)	O4−Cd1−O12	85.9(1)
N1−Cd1−O11	92.9(2)	O1A−Cd1−O11	94.7(1)
O4−Cd1−O11	92.5(1)	O12−Cd1−O11	175.1(2)
N1−Cd1−O3	84.0(1)	O1A−Cd1−O3	135.3(1)
O4−Cd1−O3	53.4(1)	O12−Cd1−O3	91.3(1)
O11−Cd1−O3	84.0(1)	N1−Cd1−O2A	87.7(1)
O1A−Cd1−O2A	53.3(1)	O4−Cd1−O2A	135.4(1)
O12−Cd1−O2A	90.8(2)	O11−Cd1−O2A	93.6(1)
O3−Cd1−O2A	171.1(1)	O8B−Cd2−N6	130.7(2)
O8B−Cd2−O5	86.9(2)	N6−Cd2−O5	142.3(2)
O8B−Cd2−O9	89.8(2)	N6−Cd2−O9	89.8(2)
N5−Cd2−O9	86.8(2)	O8B−Cd2−O10	88.3(2)
N6−Cd2−O10	94.9(1)	O5−Cd2−O10	88.6(1)
O9−Cd2−O10	175.1(1)	O8B−Cd2−O6	140.5(2)
N6−Cd2−O6	88.7(1)	O5−Cd2−O6	54.4(1)
O9−Cd2−O6	95.3(2)	O10−Cd2−O6	83.4(2)

[a] Symmetry codes: (A) $x + 1/2, y + 1/2, z$; (B) $x + 1/2, y - 1/2, z$.

Table 7. Selective Bond Lengths (Å) and Angles (deg) for Complex **9**[a]

Cd1−N7	2.328(3)	Cd1−O10	2.355(3)
Cd1−N6	2.376(3)	Cd1−O8	2.396(2)
Cd1−O6	2.405(3)	Cd1−O5	2.407(3)
Cd1−O7	2.411(2)	Cd2−N1A	2.337(3)
Cd2−O9	2.322(2)	Cd2−N12B	2.345(3)
Cd2−O2	2.406(3)	Cd2−O3	2.454(2)
Cd2−O1	2.441(2)	Cd2−O4	2.409(2)
O1−C28	1.252(4)	O2−C28	1.245(4)
O3−C33	1.245(4)	O4−C33	1.241(4)
O5−C38	1.231(4)	O6−C38	1.221(4)
O7−C29	1.232(4)	O8−C29	1.240(4)
N7−Cd1−O10	83.9(1)	N7−Cd1−N6	166.0(1)
O10−Cd1−N6	85.4(1)	N7−Cd1−O8	90.24(9)
O10−Cd1−O8	91.48(9)	N6−Cd1−O8	80.94(9)
N7−Cd1−O6	97.1(1)	O10−Cd1−O6	135.1(1)
N6−Cd1−O6	97.0(1)	O8−Cd1−O6	133.26(9)
N7−Cd1−O5	92.2(1)	O10−Cd1−O5	82.3(1)
N6−Cd1−O5	95.4(1)	O8−Cd1−O5	173.0(1)
O6−Cd1−O5	52.9(1)	N7−Cd1−O7	96.6(1)
O10−Cd1−O7	145.05(9)	N6−Cd1−O7	86.95(9)
O8−Cd1−O7	53.61(8)	O6−Cd1−O7	79.66(9)
O5−Cd1−O7	132.5(1)	O9−Cd2−N1A	86.8(1)
O9−Cd2−N12B	82.8(1)	N1A−Cd2−N12B	169.3(1)
O9−Cd2−O2	142.33(9)	N1A−Cd2−O2	93.6(1)
N12B−Cd2−O2	93.4(1)	O9−Cd2−O4	139.04(9)
N1A−Cd2−O4	96.7(1)	N12B−Cd2−O4	92.6(1)
O2−Cd2−O4	78.39(9)	O9−Cd2−O1	89.2(1)
N1A−Cd2−O1	85.1(1)	N12B−Cd2−O1	92.6(1)
O2−Cd2−O1	53.48(9)	O4−Cd2−O1	131.79(9)
O9−Cd2−O3	85.76(9)	N1A−Cd2−O3	96.88(9)
N12B−Cd2−O3	84.52(9)	O2−Cd2−O3	131.35(9)
O4−Cd2−O3	53.28(8)	O1−Cd2−O3	174.44(9)

[a] Symmetry codes: (A) $-x + 2, -y - 1, -z + 1$; (B) $-x + 1, -y + 1, -z$.

extended through both tp and bpt linkers. Remarkably, they are entangled in the crystalline lattice to result in an unprecedented 3-D polythreaded architecture through the intercalation of the bpt side arms from the 1-D patterns into the grids of the 2-D sheets (see Figure 6). More details are discussed in our previous Communication.[13a]

{[Cd(bpt)(tp)(H$_2$O)]$_2$(DMF)$_{1.5}$(H$_2$O)}$_n$ (8) and {[Cd$_2$(bpt)$_2$(tp)$_2$(H$_2$O)(DMF)]·2DMF}$_n$ (9). The network strucutres of MOFs **8** and **9** are essentially similar, although they crystallize in space groups $P2_1/n$ and $P\bar{1}$, respectively. In the asymmetric unit of **8**, there are two independent [Cd(bpt)(tp)(H$_2$O)] subunits, whereas, for **9**, the asymmetric coordination unit is assigned as [Cd$_2$(bpt)$_2$(tp)$_2$(H$_2$O)(DMF)], which contains two independent Cd^{II} centers (see Figure 7a). Each Cd^{II} ion in **9** is heptacoordinated, showing a distorted pentagonal-dipyramidal geometry (see Table 7 for details). The coordination sphere of Cd1 is defined by five oxygen atoms from a pair of tp and one DMF, as well as two nitrogen atoms from bpt. The environment around Cd2 is similar to that of Cd1 except that the DMF molecule is replaced by a water ligand. The corresponding Cd−N and Cd−O bond distances are comparable in the structures of **8** and **9**. As for the 2-D corrugated coordination networks in **8** and **9**, both of them result from the extension of metal coordination via tp and bpt connectors, as shown in Figure 7b and 7c, respectively. However, their structural discrepancy rests with the relative disposition of bpt around the Cd^{II} centers (apart from the different solvent ligands). In the structure of **8**, two unique [Cd(bpt)(tp)(H$_2$O)]$_n$ frameworks are similar, with each pair of bpt molecules around the same Cd^{II} ion taking a *syn*-arrangement. Along the [010] prolonged direction of the [Cd(tp)]$_n$ chain, the bpt ligands have a sequence of AA′AA′ (2-fold screw operation). However, in the network of **9**, the paired bpt ligands around each Cd^{II} take a trans style, and along the [Cd(tp)]$_n$ direction of [$\bar{3}$21], two distinct types of bpt ligands have a sequence of A(−A)B(−B) (centrosymmetry operation). As a result, a 2-fold parallel interpenetrating framework (see Figure 7d) similar to that of **8**[13a] is also observed for **9**, which is fixed by N5−H5A···O6 interactions,

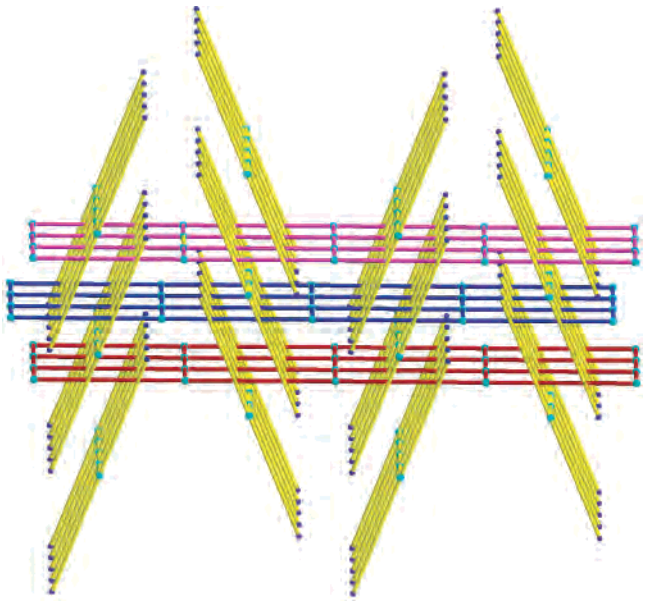

Figure 6. Schematic representation of **7** showing the interdigitated 3-D polythreading architecture consisting of the 1-D chains (yellow) and 2-D layers (magenta, blue, and red). The ip and bpt linkers are simplified as rods for clarity.

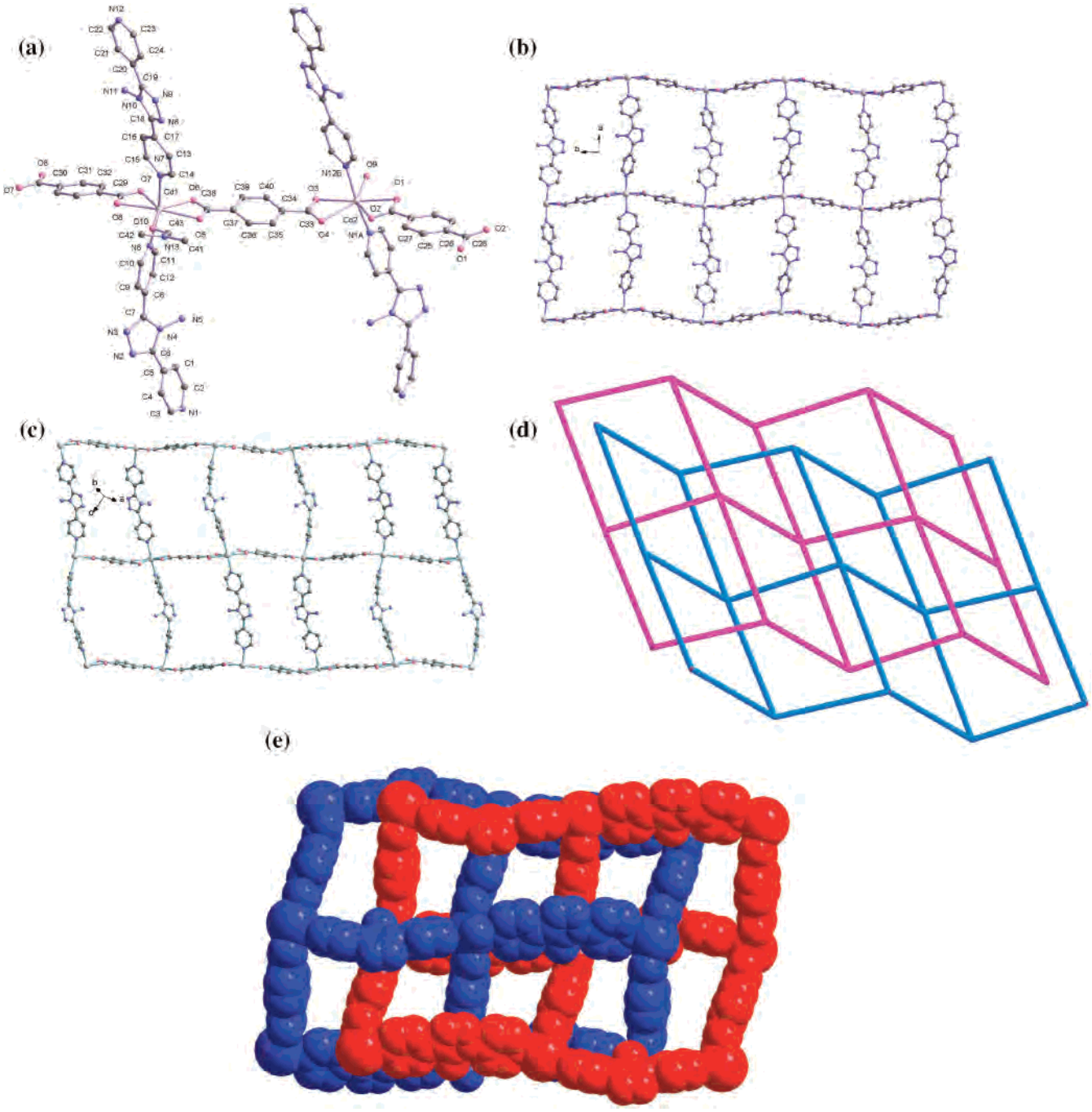

Figure 7. (a) Portional view of **9** with atom labeling of the asymmetric unit and metal coordination. Symmetry codes are listed in Table 7. The lattice DMF molecules are omitted for clarity. (b) Perspective view of the 2-D coordination layer for **8**. (c) Perspective view of the 2-D coordination layer for **9**. (d) Schematic representation of the parallel interpenetrating (4,4) networks in **9**. The ip and bpt linkers are simplified as rods for clarity. (e) Space-filling view of the interpenetration of two coordination layers in **9**, displaying the distorted square voids. The included guest solvents are omitted for clarity.

and these interpenetrating arrays are further extended to a 3-D architecture via O9−H9A···O1 contacts (see Table S1 for details). However, the cavities in the porous structure of **9** (see Figure 7e) are more distorted and relatively larger (a volume of 1090 Å^3, 40.9%/unit cell), compared with that of **8** (a volume of 1500 Å^3, 28.8%/unit cell). This may result in their distinct adsorption/desorption properties of the guest solvents as described below.

Structural Diversity of MOFs 1−9. It is noteworthy that a variety of framework structures can be achieved on the basis of the choice of the phenyl dicarboxylate isomers with differently oriented carboxyl groups as building blocks and the metal ions. In MOFs **1**−**9**, these dicarboxylate isomers exhibit several coordination patterns as illustrated in Scheme 1, in which the carboxylate groups can adopt the unidentate, chelating, and bridging modes, respectively. Generally, the bpt ligand behaves as the uniform bidentate connector in all these coordination networks but partial monodentate in **8**. Thus, the phenyl dicarboxylate isomers varied in the assembled process will be mostly responsible for structural diversity of MOFs **1**−**9**, especially when a given metal center is available. For example, with regard to the Cd^{II} MOFs **2**,

Scheme 1

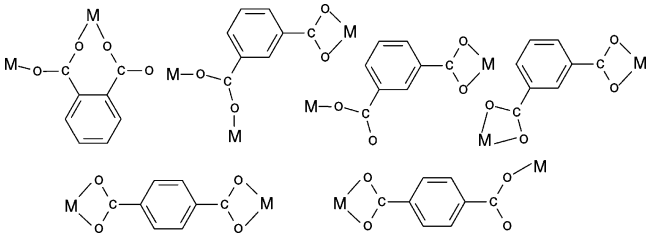

6, and **8** (or **9**) in this series of framework materials, along with the variation of the phenyl dicarboxylate building blocks (from pa and ip to tp), their network arrays are changed from 2-D isolated layers (4^4 topology) and 2-D interpenetrating bilayers ($8^2.10$ topology) to 2-D interpenetrating layers (4^4 topology). This is also comparable for the Co^{II} MOFs **1** and **3**. On the other hand, the choice of metal centers may also play a significant role on the binding fashions of the dicarboxylate isomers as well as the resultant extended networks of MOFs. As a matter of fact, most of the carboxylate groups behave as unidentate and chelating ligands. Each metal ion in isomorphic MOFs **1** and **2** forms a 7-membered chelated ring with two adjacent carboxylate groups due to the smallest separation of them in the three isomers, and this should be ascribed to a ligand-directed assembly. However, the ip and tp linkers with two separated carboxylate groups can be considered as a bent or a linear building block, respectively. For ip-containing MOFs **3**−**6**, three coordination fashions of ip are observed and, interestingly, four different types of 2-D frameworks are generated relying on the metal centers. The network structures of **7** and **8** (or **9**) are also metal-controlled, and notably, the unique 3-D polythreaded architecture is formed in the case of the Cu^{II} MOF **7**. Nevertheless, from the viewpoint of crystal engineering, we can generally discover that in all these structures the dicarboxylate isomers link the metal centers to form 1-D chains or ribbons, and their final structural discrepancy comes from the further extension of these 1-D arrays by bpt connectors in different directions (referring typically the structures of MOFs **3** and **5**), which however cannot be accurately forecasted at this stage.

Thermal Stability of MOFs 1−**9**. The thermal stability of these new crystalline materials has been investigated by thermogravimetric analysis experiments of mass loss. The TGA curves of **1** and **2** are similar due to their isostructural nature. The first weight loss of 7.23% (calcd: 7.24%) in the range 126−221 °C for **1** (101−165 °C for **2**: obd, 6.34%; calcd, 6.54%) is attributed to removal of the lattice and coordination water molecules (peaking at 208 °C for **1** and 154 °C for **2**). The remaining substance is stable up to 248 °C for **1** (228 °C for **2**), with that weight loss occurring in three consecutive steps (peaking at 191, 420, and 701 °C for **1** and 294, 378, and 552 °C for **2**), which does not stop until heating ends at 800 °C. The TGA curve of **3** shows a weight loss of 10.76% in the range 25−75 °C (calcd: 10.50%, peaking at 62 °C), corresponding to expulsion of three lattice water molecules. The main framework remains intact until it is heated to 409 °C, and then weight loss occurs in three consecutive steps (peaking at 423, 541, and 707 °C) and does not stop until heating to 800 °C. For **4**, weight loss of the lattice DMF and water molecules (obsd, 34.43%; calcd, 34.76%) is observed in the range 25−360 °C (peaking at 81, 109, 172, and 313 °C). With that, decomposition of the residuary components occurs with two steps of weight loss (peaking at 433 and 523 °C) and stops at 590 °C. For **5**, weight loss of two lattice DMF molecules (obsd: 13.05%) occurs in the range 25−300 °C (calcd: 13.52%, peaking at 285 °C), and decomposition of the coordination framework supervenes with two steps of weight loss (peaking at 353 and 409 °C), which does not end until heating to 800 °C. In the TGA curve of **6**, the weight losses in the ranges 25−183 and 193−289 °C (obsd: 9.85% and 3.79%) indicate release of the lattice and two coordinated aqua molecules (calcd: 11.12% and 3.71%, peaking at 61 and 276 °C). With that, pyrolysis of the residual structure occurs with a series of consecutive steps of weight loss (peaking at 347, 389, 416, and 522 °C), which does not stop until heating to 800 °C. As for **7**, elimination of the lattice water molecules is not observed individually. It undergoes three consecutive steps of weight loss upon reaching 90 °C (peaking at 298, 374, and 436 °C), which does not stop until heating to 800 °C. With regard to **8**, all solvents are released from 86 to 280 °C (peaking at 50 and 150 °C), as revealed by a total weight loss of 11.64% (calcd: 10.70%). The host framework starts to decompose when heating beyond 340 °C with two steps of weight loss (peaking at 399 and 506 °C), which does not stop until heating to 800 °C. The TGA curve of **9** shows exclusion of the captured DMF guests with a weight loss of 11.87% (calcd: 11.52%) in the temperature range 60−300 °C (peaking at 174 °C). Beyond 325 °C, the residual framework begins to decompose with two steps of weight loss (peaking at 401 and 510 °C), which does not stop until heating to 800 °C.

Photoluminescence Properties. Metal−organic frameworks constructed from d^{10} metal centers and conjugated organic linkers are promising candidates for hybrid photoactive materials with potential applications such as light-emitting diodes (LEDs).[25] These crystalline solids usually display high thermal stability and regulable photoluminescence properties. Therefore, solid-state emission spectra of the Zn^{II} and Cd^{II} MOFs **2**, **5**, **6**, **8**, and **9** have been investigated at room temperature, as depicted in Figure 8 (the luminescence emission of **9** is almost the same as that of **8**, which thus is not shown). Excitation of the microcrystalline sample of **2** at 320 nm produces an intense luminescence with the peak maximum at 362 nm. For MOFs **5**, **6**, and **8**, two intense emission peaks occur at 388/400, 393/420, and 392/410 nm, respectively (λ_{ex} = 320 nm). Additionally, their emission spectra also display the similar shoulder peaks at ca. 362 nm. To further analyze the nature of these emission bands, the photoluminescence property of the ligand bpt has also been explored. The free bpt molecule exhibits a weak and an intense emission peaks at 362 and

(25) (a) Zheng, S.-L.; Yang, J.-H.; Yu, X.-L.; Chen, X.-M.; Wong, W.-T. *Inorg. Chem.* **2004**, *43*, 830. (b) Wang, R.-H.; Han, L.; Jiang, F.-L.; Zhou, Y.-F.; Yuan, D.-Q.; Hong, M.-C. *Cryst. Growth Des.* **2005**, *5*, 129.

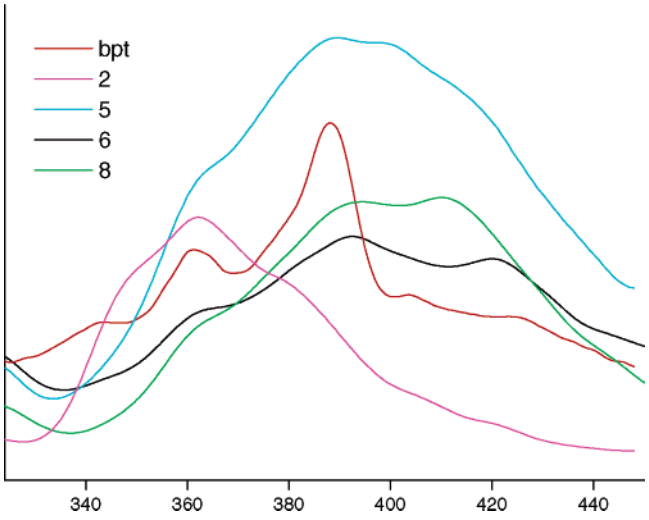

Figure 8. Solid-state fluorescence emissions recorded at room temperature for bpt (red) and MOFs **2** (magenta), **5** (cyan), **6** (black), and **8** (green).

388 nm (λ_{ex} = 320 nm), respectively (see Figure 8). Thus, we can presume that the emission peaks at 362 nm for all these polymeric complexes should originate from the intraligand $\pi \rightarrow \pi^*$ transitions of bpt. With respect to MOFs **5**, **6**, **8**, and **9**, the fluorescence peaks appeared around 390 nm should also be ascribed to the ligand-centered transitions, and the small red shift in the case of **6**, **8**, and **9**, compared with that of the bpt ligand, is due to the increase of conjugation upon metal coordination. Furthermore, the added peaks at above 400 nm for these complexes (especially for **6**, **8**, and **9** that are more evident) may be attributed to the ligand-to-metal charge transfer (LMCT) bands.

Guest Desorption/Adsorption Behaviors of MOFs 8 and 9. As described in the structural section, MOFs **8** and **9** possess similar porous frameworks despite interpenetration of the layered networks. Also similarly, the results of TGA experiments suggest that the included solvent molecules could be excluded from the crystalline lattices in both cases upon heating, before decomposition of the host structures occurs. Thus, an investigation on removal and reintroduction of the guest solvents has been carried out for MOFs **8** and **9** with the following procedure. A freshly ground sample (ca. 100 mg) was placed inside a vacuum oven at 280 °C over a period of 8 h. The sample shows a weight loss that is consistent with removal of all included lattice solvents. For both cases, the XRPD patterns recorded at this point display significant shifts of the main diffraction peaks compared with those of the original materials. This result suggests that the structures of the desolvated solids of MOFs **8** and **9** are changed due to release of the guest molecules although the periodicity is still (at lease partially) maintained. Then, the desolvated samples were soaked in DMF for 24 h to regain the guest molecules. Significantly, the XRPD patterns of the resultant solids suggest that the structure of **8** is regenerated after this desorption/adsorption cycle, and however for **9**, the desolvated sample is unchanged after the reintroduction process of guest solvents. The XRPD patterns for **9** under different conditions are given in Figure S2 (see Supporting Information for details), and those for **8** are archived in our previous publication.[13a] Different guest desorption/adsorption behaviors of MOFs **8** and **9** should be attributed to the subtle differentiation of their crystalline lattices, as discussed above.

Conclusions

We present here a new family of metal−organic frameworks generated from mixed-ligand systems of three phenyl dicarboxylate isomers and bpt under the coordinative-driven assembly. In general, the phenyl dicarboxylate isomers with different orientation/disposition of the carboxylate groups do play a dominating role in the construction of these crystalline materials; that is, they behave as linear (tp) or angular (pa and ip) building blocks imposing on the final structural arrays. Together with the secondary N-donor connector bpt, diverse and interesting coordination architectures upon metal complexation could be produced readily. These results undoubtedly discover the isomeric effect of the bridging ligands in molecular tectonics of metal−organic frameworks, and in this context, the series of Cd^{II} MOFs **2**, **6**, and **8** are representative examples. Also as expected, the metal centers are critical in the direction of these coordination networks. Accordingly, our present findings will further enrich the crystal engineering strategy and offer the possibility of controlling the formation of the desired network structures. On another aspect, this work prompts us to achieve more functional crystalline solids via such a reliable synthetic route by employing mixed-ligand bpt and other aromatic multicarboxylate isomers as spacers, and further efforts on this perspective are underway.

Acknowledgment. This research was financially supported by the National Natural Science Foundation of China (Grant Nos. 20401012 and 20671071), the National Fundamental Research Project of China (Grant No. 2005CCA01200), the Key Project of Chinese Ministry of Education (Grant No. 205008), and Tianjin Normal University.

Supporting Information Available: X-ray crystallographic files (CIF), tables for pertinent hydrogen-bonding parameters of **1**, **4**, **5**, and **9** (Table S1) and selective bond geometries of **2** (Table S2), X-ray powder diffraction (XRPD) patterns for **1**−**9** (Figures S1 and S2), and a schematic view showing the network connectivity in **3** and **5** (Scheme S1). This material is available free of charge via the Internet at http://pubs.acs.org.

IC062098+